Volume 849, 16 August 2024

ISSN 0009-2614

CHEMICAL PHYSICS LETTERS

Frontier research in molecular sciences, materials and biological systems

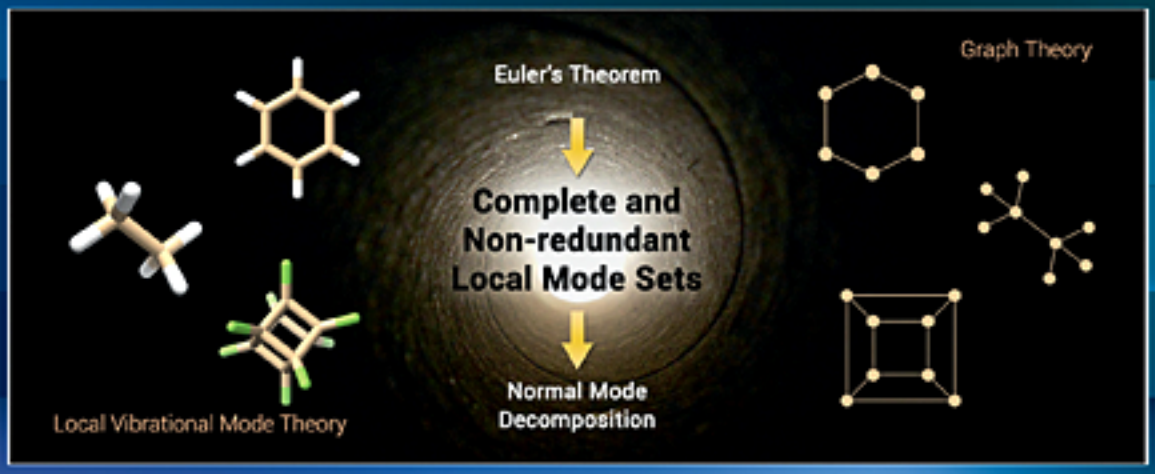

www.elsevier.com/locate/cplett

MATEUS QUINTANO, RENALDO T. MOURA JR. AND ELFI KRAKA
ARTICLE NUMBER: 141416, IN THIS ISSUE

Chemical Physics Letters 849 (2024) 141416

Contents lists available at ScienceDirect

Chemical Physics Letters

journal homepage: www.elsevier.com/locate/cplett

Frontiers article

Local vibrational mode theory meets graph theory: Complete and non-redundant local mode sets

Mateus Quintano [a], Renaldo T. Moura Jr. [a,b], Elfi Kraka [a,*]

[a] Computational and Theoretical Chemistry Group (CATCO), Department of Chemistry, Southern Methodist University, Dallas, TX 75275, USA
[b] Department of Chemistry and Physics, Center of Agrarian Sciences, Federal University of Paraiba, Areia, PB 58397-000, Brazil

HIGHLIGHTS

- Presentation of a topological description of complete and non-redundant local mode sets.
- Generalization of the local mode parameter count formulas employing Euler's theorem.
- Substantiation of our recent and original protocol of local mode analysis, LModeAGen.

GRAPHICAL ABSTRACT

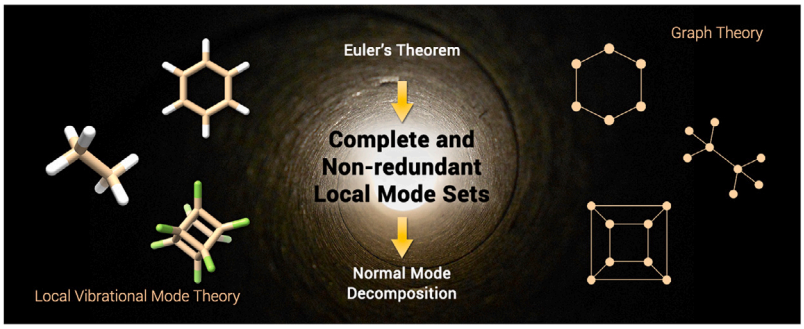

ARTICLE INFO

Keywords:
Vibrational spectroscopy
Topology
Local mode analysis
Euler's polyhedral formula

ABSTRACT

This Frontiers Article introduces a unique perspective on the well-established concept of completeness in a chemically meaningful set of non-redundant local vibrational modes. By utilizing graph theory, we demonstrate how this concept naturally arises when Euler's theorem is fulfilled in molecular graphs of tree, cycle, and polyhedral types. This significantly advances our understanding of topology, leading to a new interpretation for deriving such a set. A key aspect of the local vibrational mode theory is the decomposition of normal modes into local mode contributions, which provides a powerful approach for analyzing vibrational spectra. This however requires a complete and meaningful set of non-redundant local vibrational modes, as demonstrated for the IR spectra of both non-zwitterionic and zwitterionic forms of glycine, the cubane and perfluorocubane pair, and the Ar–benzene dimer. The mathematical concept is put to the test by applying our counting formulas for complete and non-redundant local mode sets to a series of organic molecules with increasing complexity.

1. Introduction

Vibrational spectroscopy serves as a potent tool for unraveling intricate details of the electronic structure of a molecule and its chemical bonds [1,2]. It is customary to link measured or calculated vibrational frequencies with distinct patterns of molecular vibration. Following the Wilson GF formalism [3,4], to each vibrational frequency, also called normal mode frequency, a normal mode vector can be assigned, which describes the corresponding molecular vibration. However, normal vibrational modes are generally delocalized within the molecular system, which poses interpretation challenges and also questions the popular use of normal vibrational frequencies and related normal mode force constants as bond strength measure [1,2]. In contrast, local vibrational modes derived from our local vibrational mode (LVM) theory [1,2,5] are confined within specific molecular fragments, recently referred to in the literature as "diatomics-within-molecules" [6]. They provide a

* Corresponding author.
E-mail address: ekraka@gmail.com (E. Kraka).

https://doi.org/10.1016/j.cplett.2024.141416
Received 11 April 2024; Received in revised form 7 June 2024; Accepted 10 June 2024
Available online 12 June 2024

better fit for describing the vibrational properties associated with the internal coordinates of a molecule, such as bonds, angles, and dihedral angles, as well as interpreting vibrational spectra. The importance of internal coordinates has been highlighted in the literature [7–14]. In his seminal work, Decius provided an elegant mathematical demonstration that bonds, angles, and dihedral angles form a topologically complete set [7], laying one of the foundations for the present work.

Besides providing a quantitative measure of the intrinsic strength of a chemical bond or weak chemical interaction [1,2,15], another key feature of the LVM theory is the characterization of normal mode (CNM) procedure, which decomposes each normal vibrational mode into local mode contribution, physically based on an adiabatic connection scheme (ACS), i.e., the one-to-one correspondence between a non-redundant set of local vibrational modes and the corresponding set of normal vibrational modes [16]. Both tools, CNM and ACS, integrated within LVM, have proven to provide a unique instrument for a comprehensive analysis and interpretation of vibrational spectra, as documented in the literature [2,17–22], predating a recent study that claims to have introduced the concept of normal mode decomposition [23]. The method [24] employed in that study [23] for quantifying molecular vibrations has been identified in the 1990s to be highly reliant on the chosen set of internal parameters used to define the geometry of the molecule [25]. In contrast, local vibrational modes remain unaffected by the choice of parameter set, highlighting that variations observed in the calculated properties of local vibrational modes provide valuable insights into the electronic structure of the fragments, rather than being influenced by the selection of internal parameters [2,25]. For an overview of LVM, the reader is referred to Ref. [2]. The different use of the term 'local mode' in the literature, which should not be confused with LVM, is discussed in Ref. [1]. Among the different local-mode approaches, the one that incorporates anharmonicity effects [26,27] is particularly appealing and has been of recent interest [28,29]. However, since our approach is static rather than dynamic, such a comparison falls outside the scope of this Frontiers Article. Some recent applications of the LVM theory range from large systems of biological interest [30–33] to problems within the realm of relativistic quantum chemistry [34]. Furthermore, an enhanced implementation of the LVM theory for analyzing 2D/3D periodic systems has been recently released [35].

Recently, we introduced a novel protocol, LModeAGen [19], designed for the automatic generation of local mode parameters. This protocol is capable of producing a complete and non-redundant set of N_{vib} chemically meaningful local vibrational modes required for ACS and CNM, where $N_{vib} = 3N - N_{tr}$. Here, N_{tr} denotes the translational and rotational degrees of freedom, which amounts to 5 for linear and 6 for non-linear molecules composed of N atoms. LModeAGen utilizes molecular connectivity and marks a significant advancement, offering a solution to the challenges associated with unphysical parameters and addressing the intricacies of systems with high symmetry, cyclic structures (without disregarding bonds and disrupting symmetry), and larger molecular complexes extending beyond small and mid-sized molecules [19]. LModeAGen [19] can be integrated with the generalized subsystem vibrational analysis (GSVA) [36,37] for QM/MM systems. This integration allows for the extraction of intrinsic fragmental vibrations from any fragment/subsystem within the whole system, achieved through the evaluation of the corresponding effective Hessian matrix [36,37]. Notably, LModeAGen has undergone successful testing in various applications [2,18–21], always numerically satisfying the total amount of local mode parameters that ensures meaningful local mode analysis data [16]. For further details on how LModeAGen selects internal coordinates, please refer to Ref. [19].

The study of molecules through the lens of topology can shed light on chemical properties and has attracted increasing interest [38–53]. The intricacies of high symmetry such as that of rings [54,55] and polyhedral structures such as cubane [56], buckminsterfullerene [57], or the recently synthesized electron cage, perfluorocubane [58], serve as an inspiration for contemplating the chemical aesthetics and mark a significant milestone in synthetic chemistry [59]. As elaborated below, graphs in which the edges only intersect at their endpoints are categorized as planar graphs [47,52,60–62]. However, within the realm of molecular structures, it is worth noting that certain shapes can manifest non-trivial topological intricacies [51–53,63–71].

In this Frontiers Article, we aimed to address the following issues:

- Previous efforts in tackling the counting problem of complete and non-redundant sets of local vibrational modes have provided useful formulas ensuring meaningful local mode results [16,19]. However, none have attempted to generalize these approaches to encompass molecules from a broader perspective.
- What has been missing is an intuitive realization that views molecules as connected graphs, thereby taking a significant step towards recognizing that the count of bond local mode parameters should adhere to Euler's theorem [60–62]. Essentially, there has been a lack of a clear connection between local vibrational mode theory and graph theory.
- This connection has the potential to merge vibrational spectroscopic and topological concepts, offering a broader perspective that includes various structural types, such as open-chain, cyclic, and even cage structures, which are systems of growing interest in recent studies [42,45,58,59,72–80].

In addition, a demonstration of LVM is provided to illustrate the identification of localization and a penetrating look into the subtleties of normal vibrational modes, as well as to gauge bond strength through the local force constant. Fig. 1 depicts the molecular systems selected for this study, encompassing: acetylene (**1**), ethane (**2**), glycine (**3**), benzene (**4**), bicyclo[2.2.2]octane (**5**), cubane (**6**), perfluorocubane (**7**), buckminsterfullerene (**8**), and Ar–benzene (**9**). We have chosen examples to represent molecular systems characteristic of tree graphs (**1**–**3**), cycle graphs (**4** and **5**), and polyhedral graphs (**6**–**9**). System **3** has been included due to its relevance in astrochemistry [81–84], as well as the anticipated distinctions in the infrared spectra acquired for amino acids in their neutral and zwitterionic forms [85]. Considering that a molecular graph reflects the topological characteristics of a system's charge distribution [86], it is evident that the concepts explored in our work extend beyond the realm of organic molecules.

2. Methodology

This section serves to provide context for the integration of graph theory concepts into the framework of local vibrational mode theory. By doing so, it lays the foundation for understanding the novel approach employed to take local mode analysis from a different perspective. Following this contextualization, we delve into the core components of local mode analysis, offering an exploration that is showcased in the subsequent section. This all should come later.

2.1. Computational details

Electronic structure calculations were conducted using the Gaussian 16 quantum chemistry program [87] at the density functional theory level. To ensure accuracy, an ultra-fine grid integration and a tight convergence criterion were applied during the self-consistent field procedure. The equilibrium geometries for the examples **1**–**9**, along with the subsequent Hessian matrix and associated normal vibrational modes, were obtained using the ωB97X-D functional [88] in conjunction with Dunning's aug-cc-pVTZ basis set [89,90]. The Polarizable Continuum Model (PCM) [91], employing water as the solvent, was utilized to achieve the equilibrium geometry for the zwitterionic form of glycine (**3**). All the geometries were visualized using UCSF ChimeraX [92].

The automatic generation of non-redundant and complete sets of local vibrational modes was accomplished through our newly developed

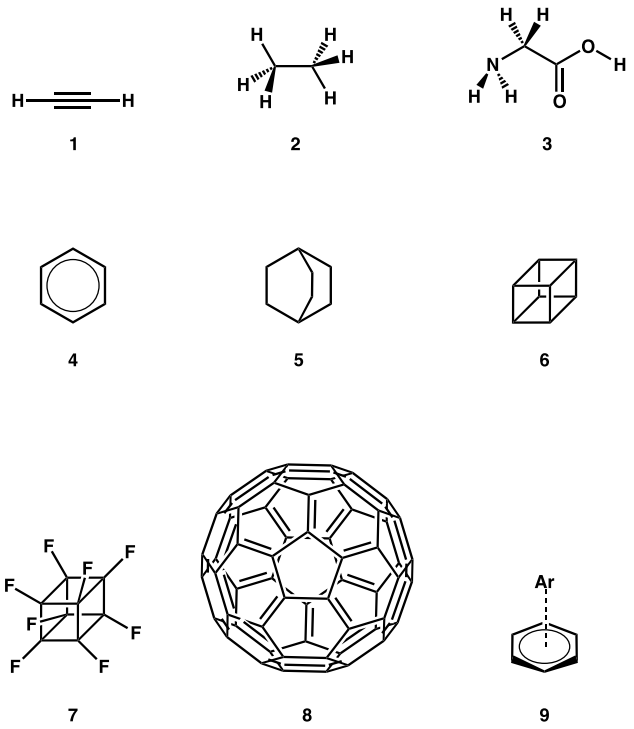

Fig. 1. Illustration of the examples selected for this work.

LModeAGen protocol [19]. Subsequently, the local mode analysis was conducted using the standalone LModeA package [93].

The constants a and b mentioned in Eq. (20) were determined for C–C bonds based on examples **1** and **2**, corresponding to BSO n values of 3 and 1, respectively.

2.2. GF method

The matrix theory of normal vibrational modes described in this section is known as the GF method [3,4]. The Lagrangian $\mathcal{L}$ of a polyatomic molecule with N atoms that vibrates harmonically can be generalized by the following matrix formulation

$$\mathcal{L} = \frac{1}{2}\dot{\mathbf{q}}^{\dagger}\mathbf{G}^{-1}\dot{\mathbf{q}} - \frac{1}{2}\mathbf{q}^{\dagger}\mathbf{F}^{q}\mathbf{q} \tag{1}$$

The $N_{vib} \times N_{vib}$ matrices $\mathbf{G}$ and $\mathbf{F}^q$ are the Wilson G matrix and the Hessian in internal coordinates q, respectively. The internal coordinate vector $\mathbf{q}$ can be defined as a linear transformation $\tilde{\mathbf{D}}$ of the normal coordinate vector $\mathbf{Q}$ as follows

$$\mathbf{q} = \tilde{\mathbf{D}}\mathbf{Q} \tag{2}$$

The normal vectors $\tilde{\mathbf{d}}_{\mu}$ ($\mu = 1, \ldots, N_{vib}$) in internal coordinates form the columns of the matrix $\tilde{\mathbf{D}}$.

The vibrational secular equation expressed in internal coordinates is given by

$$\mathbf{F}^{q}\tilde{\mathbf{D}} = \mathbf{G}^{-1}\tilde{\mathbf{D}}\mathbf{\Lambda} \tag{3}$$

The following equality involving the identity matrix $\mathbf{I}$ is true:

$$\tilde{\mathbf{D}}^{\dagger}\mathbf{G}^{-1}\tilde{\mathbf{D}} = \mathbf{I} \tag{4}$$

The diagonal matrix $\mathbf{\Lambda}$ contains N_{vib} eigenvalues λ_{μ}, which give N_{vib} frequency values ω_{μ} (in the units of cm^{-1}) associated with each normal coordinate Q_{μ}:

$$\omega_{\mu} = \frac{1}{2\pi c}\lambda_{\mu}{}^{1/2} \tag{5}$$

with c being the speed of light in vacuum. In other words, the set of diagonal elements λ_{μ} of the matrix $\mathbf{\Lambda}$ gives rise to the vibrational spectrum of a polyatomic molecule.

The Wilson B matrix, a $N_{vib} \times 3N$ rectangular matrix comprising the first derivatives of the internal coordinates q_n ($n = 1, \ldots, N_{vib}$) with respect to the Cartesian coordinates x_i ($i = 1, \ldots, 3N$) as its elements B_{ni}, establishes the link between internal and Cartesian coordinates [4]:

$$\mathbf{q} = \mathbf{B}\mathbf{x} \tag{6}$$

$$\mathrm{B}_{ni} = \frac{\partial q_n}{\partial x_i} \tag{7}$$

The pseudo-inverse matrix of $\mathbf{B}$ is the matrix $\mathbf{C}$ [1]:

$$\mathbf{C} = \mathbf{M}^{-1}\mathbf{B}^{\dagger}\mathbf{G}^{-1} \tag{8}$$

$\mathbf{M}$ is the mass matrix, a $3N \times 3N$ matrix containing each atomic mass three times to account for the motion in the x, y and z directions.

Renormalization of $\tilde{\mathbf{D}}$, via the diagonal matrix $\mathbf{M}^R$ of reduced mass elements m_{μ}^R, according to

$$\mathbf{D} = \tilde{\mathbf{D}}(\mathbf{M}^R)^{1/2} \tag{9}$$

leads to

$$\mathbf{D}^{\dagger}\mathbf{G}^{-1}\mathbf{D} = \mathbf{M}^R \tag{10}$$

$$\mathbf{D}^{\dagger}\mathbf{F}^{q}\mathbf{D} = \mathbf{K} \tag{11}$$

by rewriting Eqs. (3) and (4), respectively. $\mathbf{D}$ is the column-wise collection of the normal vectors $\mathbf{d}_{\mu}$ and $\mathbf{K}$ is the diagonal normal force constant matrix, that is, $\mathbf{K} = \mathbf{F}^{Q}$. Another bridge between internal and Cartesian coordinates is given by

$$\mathbf{F}^{q} = \mathbf{C}^{\dagger}\mathbf{F}^{x}\mathbf{C} \tag{12}$$

$$\mathbf{L} = \mathbf{C}\mathbf{D} \tag{13}$$

Evidently, $\mathbf{L}$ collects the normal vectors $\mathbf{l}_{\mu}$ in its columns.

Left multiplication of Eq. (2) by $\tilde{\mathbf{D}}^{\dagger}\mathbf{G}^{-1}$ considering Eq. (4) gives

$$\mathbf{Q} = \tilde{\mathbf{D}}^{\dagger}\mathbf{G}^{-1}\mathbf{q} \tag{14}$$

In essence, normal coordinates emerge as linear combinations of internal coordinates, leading to normal vibrational modes delocalized throughout the molecule. Consequently, relying solely on normal mode frequencies and force constants becomes limited in assessing bond strength. To overcome this limitation, local vibrational modes with their respective frequencies and force constants become indispensable, as shown in the ensuing section. Additionally, the widespread delocalization hinders the tracking of subtle structural changes without a method for normal mode decomposition. Serving as a quantitative approach, CNM decomposes normal vibrational modes into local mode contributions, enabling a thorough analysis of vibrational spectra.

2.3. Local vibrational mode theory

The intricacies of local mode analysis have been extensively covered in two comprehensive feature articles [1,2]. Therefore, this section focuses on key aspects of the method. The normal vibrational modes $\mathbf{d}_n$ and the diagonal force constant matrix $\mathbf{K}$ can be utilized to calculate local mode vectors $\mathbf{a}_n$ associated with the internal coordinates q_n, as demonstrated by Konkoli and Cremer [5]:

$$\mathbf{a}_n = \frac{\mathbf{K}^{-1}\mathbf{d}_n^{\dagger}}{\mathbf{d}_n\mathbf{K}^{-1}\mathbf{d}_n^{\dagger}} \tag{15}$$

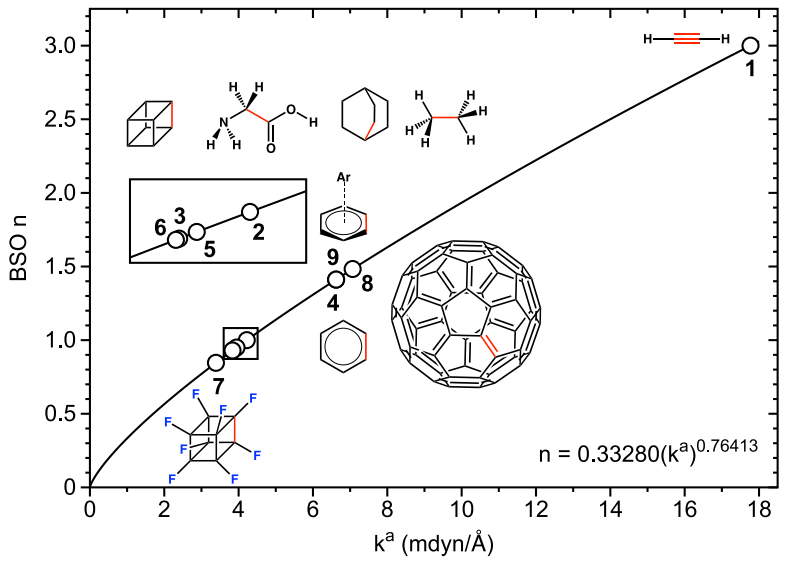

Fig. 2. Bond strength order (BSO) for C–C bonds based on local C–C force constants for examples **1**–**9** at the ωB97X-D/aug-cc-pVTZ level of theory.

It is worth noting that $\mathbf{d}_n$ and $\mathbf{K}$ can be readily obtained from standard quantum chemistry packages following a vibrational frequency calculation. The local mode vector $\mathbf{a}_n$ can be readily converted to the Cartesian coordinate space via $\mathbf{L}$ to give $\mathbf{a}_n^x$ as follows

$$\mathbf{a}_n^x = \mathbf{L}\mathbf{a}_n \tag{16}$$

The local mode force constant k_n^a, which was elucidated by Zou and Cremer as a local descriptor of the intrinsic strength of the bond or non-covalent interaction between two atoms under consideration [15], can be calculated as outlined below:

$$k_n^a = \mathbf{a}_n^\dagger \mathbf{K}\mathbf{a}_n = (\mathbf{d}_n \mathbf{K}^{-1} \mathbf{d}_n^\dagger)^{-1} \tag{17}$$

This allows for the calculation of the local mode frequency ω_n^{a}:

$$(\omega_n^{\mathrm{a}})^2 = (4\pi^2 c^2)^{-1} \frac{\mathrm{k}_n^{\mathrm{a}}}{m_n^{\mathrm{a}}} \tag{18}$$

with m_n^{a} being the local mode mass, which can be calculated in terms of the diagonal element of $\mathbf{G}$:

$$m_n^{\mathrm{a}} = \frac{1}{G_{nn}} \tag{19}$$

Rather than directly comparing the values of the local force constants, a more convenient approach for discussing larger sets of molecules is to utilize a relative bond strength order (BSO) denoted as n. These two aspects are interconnected through a power relationship, as illustrated by the following equation for a given internal coordinate on the basis of the generalized Badger rule of Cremer, Kraka, and coworkers [94,95]:

$$BSO\ n = a(k^a)^b \tag{20}$$

Under the requirement that a force constant value of zero corresponds to a BSO n value of zero, the constants a and b are computed using the k^a values of two reference compounds with known BSO n values. In other words, BSO n provides chemists with a more intuitive understanding of bond strength by linking it to the local force constant through the familiar concept of bond order.

Recently, the LVM theory has made significant progress, emerging as a robust descriptor for bond strength encompassing diverse interactions, from covalent bonds to non-covalent interactions such as hydrogen bonds, halogen bonds, tetrel bonds, and π-hole interactions [20,96–98]. For a comprehensive compilation of examples, refer to Refs. [1,2] and the references therein. Recent advancements have highlighted the effectiveness of k^a in accurately capturing packing effects and serving as a reliable indicator of bond strength for periodic systems as well, regardless of the crystal's nature [35]. Moreover, a novel metric has been introduced, the metal-ligand electronic parameter (MLEP) [99], which has found application in various studies, including the investigation of iron-ligand bonding in carboxy myoglobins and carboxy neuroglobins [100,101], as well as the assessment of non-covalent π-interactions in mutated aquomet-myoglobin proteins [30]. Additionally, our recent integration of local mode force constants into lanthanide spectroscopy has yielded fresh insights into the bonding behavior of lanthanide complexes. This approach sheds light on the inverse correlation between lanthanide-ligand strength and ligand effective polarizability, thereby advancing our understanding of lanthanide chemistry [18].

Now turning our attention to the bond strength analysis, it must be emphasized that it does not require a complete and non-redundant set. However, we included it in this section to showcase the capability of the LVM theory beyond the CNM analysis, which is showcased in the form of significant results later in this Frontiers Article. Compared with the C–C bonds in ethane (**2**) and acetylene (**1**), our findings reveal intriguing insights into the strengths of C–C bonds within the series ranging from **1** to **9** (see Fig. 2). Perfluorocubane (**7**) is distinguished by having the weakest C–C bond among all the examples considered. This observation offers a supplementary description given its electron-accepting capability as an electron cage [58,59]. This analysis highlights the diverse bond strengths within these molecular structures, with implications for their stability and reactivity. Only the non-zwitterionic form of **3** is included in Fig. 2 because PCM was utilized for the computation of the zwitterion, which represents a different level of theory compared to the rest of the BSO series.

The necessity for a spectral analysis tool capable of quantitatively assessing the individual contributions of molecular fragments to each normal vibrational mode composing the vibrational space of a molecule must be evident to anyone who has grappled with interpreting vibrational spectra using qualitative and pictorial symbols. These symbols, usually found in tiresome tables for peak assignments, denote stretching, bending, wagging, twisting, rocking, and scissoring vibrations. Normal vibrational modes generally suffer from delocalization, making it impractical to monitor subtle structural variations and changes in the surroundings of the molecule without a method for normal mode decomposition. In this context, the CNM procedure emerges as an original and powerful tool that is an integral part of the LVM theory, providing a quantitative approach for decomposing normal vibrational

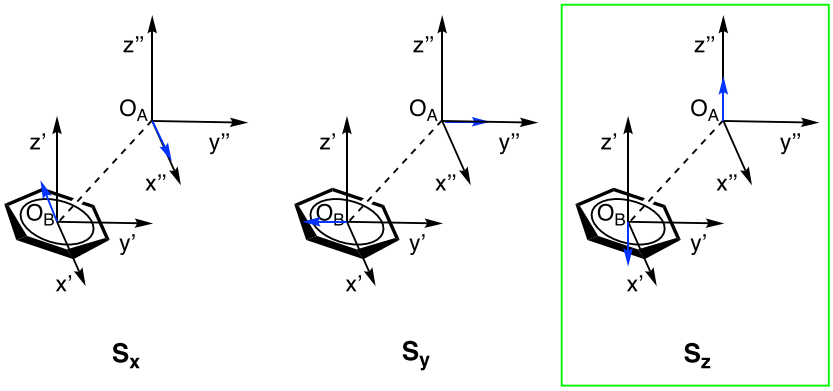

Fig. 3. The interaction between an atom A (Ar in this study) and a benzene ring B is defined as follows: O_A is the geometric center of the rotated monomer A, O_B and x′y′z′ define the standard orientation of ring B; the coordinate system x″y″z″ is derived from the original system x′y′z′ by shifting it from O_B to O_A [97]. In this study, the interaction between A and B is characterized using the framed $\mathbf{S}_z$ motion.

modes into local mode contributions. Consequently, it enables the analysis of vibrational spectra in a novel and innovative manner.

Each normal vibrational mode (corresponding to absorption peaks) can be decomposed into the percentage contributions of non-redundant local vibrational modes from a complete set using the CNM procedure on the basis of ACS, an essential component of local mode analysis. The degree of overlap, as represented by $S_{n\mu}$ [1,2,102], is defined as:

$$S_{n\mu} = \frac{\langle \mathbf{a}_n^x | \mathbf{F}^x | \mathbf{l}_\mu \rangle^2}{\langle \mathbf{a}_n^x | \mathbf{F}^x | \mathbf{a}_n^x \rangle \langle \mathbf{l}_\mu | \mathbf{F}^x | \mathbf{l}_\mu \rangle} \tag{21}$$

with $\mathbf{a}_n^x$, $\mathbf{F}^x$ and $\mathbf{l}_\mu$ being the local vibrational mode, the Hessian matrix and the normal vibrational mode in Cartesian coordinates. The percentage contribution $C_{n\mu}^{\%}$ (local mode contribution) of the local vibrational mode $\mathbf{a}_n^x$ to the normal vibrational mode $\mathbf{l}_\mu$ is then calculated as follows [102]

$$C_{n\mu}^{\%} = \frac{S_{n\mu}}{\sum_m^{N_{vib}} S_{m\mu}} 100 \tag{22}$$

A CNM plot displays normal mode decompositions, with the local mode contributions $C_{n\mu}^{\%}$ depicted as distinct components forming the bars representing normal modes in a diagram. The normal frequencies corresponding to the decomposed normal modes are shown on the plot's x-axis.

One of the advantages of LVM lies in its capability to perform local mode analysis on specific molecular fragments, such as bonds, angles, and dihedral angles, using only the necessary local mode parameters for these fragments. Moreover, any set of parameters can be utilized without altering the values of the local mode properties, highlighting the sensitivity and reliability of these properties to the electronic structure of the fragments. On the contrary, conducting CNM necessitates a complete and non-redundant set of local mode parameters. Despite the absence of a unique set due to the non-uniqueness of the choice internal coordinates, selecting parameters randomly to form a chemically meaningful set is ludicrous. The problem becomes particularly challenging for larger systems or molecules with higher structural complexity, such as polyhedral molecules. To address this challenge, we previously developed an automatic method (LModeAGen) based on molecular graphs [19]. However, a comprehensive explanation generalizing the local mode parameter count formulas to encompass the significant class of polyhedral molecules, along with a rigorous mathematical analysis based on graph theory [60–62], has been lacking. To bridge this gap, we delved deeper into graph theory, integrating Euler's polyhedral formula with Decius's seminal work [7]. This combined approach offers a solution to the problem at hand.

2.3.1. Special local modes for the Ar–benzene dimer

The π interaction between argon and benzene in Ar–benzene (**9**) has been demonstrated to possess predominantly electrostatic character [97]. Our group has previously developed, tested, and reported special local modes for describing the intermolecular π interaction between two monomers [97]. These modes have shown superior performance compared to other approaches for describing such interactions, such as the ansatz based on the six Ar–C interactions (in the Ar–benzene dimer) or the approach guided by the bond paths of the electron density [97]. Here, our endeavor was to combine the approach of these special local modes with that of the new protocol of local mode analysis, LModeAGen [19]. This adaptation was guided by the topological insights presented in this Frontiers Article, aiming to consistently achieve a complete and non-redundant local mode set for the CNM analysis of dimeric systems such as test example **9**.

Fig. 3 illustrates the methodology for obtaining a set of non-redundant local inter-monomer modes, emphasizing the establishment of a physically meaningful local inter-monomer mode (S_z) directly correlated with the interaction between the two monomers [97]. For an in-depth comprehension of this mathematical construct, readers are directed to the thorough explanation provided in Ref. [97], which falls outside the scope of this Frontiers Article.

As monomer A functions as an atom in the present work (Ar in the Ar–benzene dimer), only three specific local modes are required, given that an atom lacks rotational degrees of freedom [97]: $[3(1+N_B)-6]-(3N_B-6)=3$. Thus, the intra-monomer stretching modes along the x-, y-, and z-directions, denoted as S_x, S_y, and S_z, respectively, were utilized in this work for the first time in combination with LModeAGen [19] for the CNM analysis. Given the need for a specific adaptation alongside a topological argumentation, the reasoning behind it is elucidated as one of the results presented in this Frontiers Article.

2.4. Graph theory

The ideas discussed in the present work are based on a set of distilled mathematical concepts, as outlined below [60]:

(i) A graph $G(V, E)$ is a mathematical object comprising two sets: its vertex set V and its edge set E. In this work, v and e denote the number of vertices within V and edges within E, respectively.
(ii) The degree of a vertex v_i, denoted as $deg(v_i)$, is determined by the number of its incident edges (or neighbors).
(iii) A graph is considered connected if there is a walk (a sequence of edges) between any pair of vertices within the graph.
(iv) A graph is considered planar if it can be represented in the plane (*planar embedding* [47]) without any intersecting edges (see Fig. 4). In a planar graph, every subgraph is also planar.

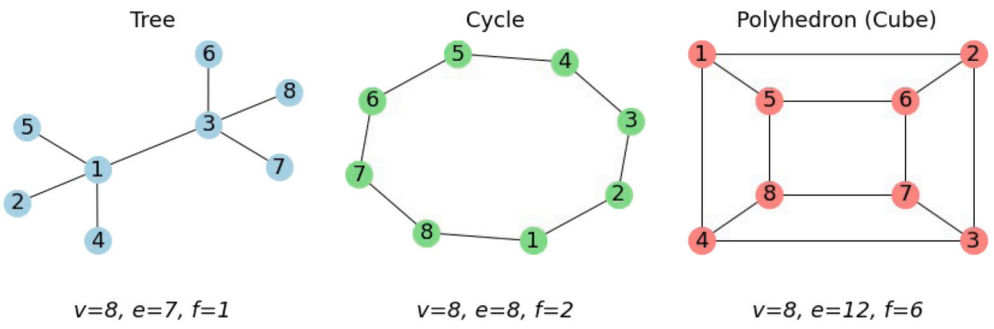

Fig. 4. Representations of a tree, cycle, and polyhedral graph, each containing v vertices, e edges and f faces.

(v) Regions known as faces emerge from the planar representation of a planar graph. The *infinite face*, which refers to the exterior region, is included in the number of faces, denoted herein as f. Ref. [61] elegantly demonstrates the emergence of the *infinite face* from the planar representation.
(vi) A cycle is a graph in which the first and last vertices are the same ($v \geq 3$).
(vii) A tree is a connected graph that always has a unique simple path between any two of its vertices [61,62]. If a graph has a cycle, it cannot be classified as a tree.
(viii) A graph is considered polygonal when it fulfills three criteria: it must be planar, connected, and each edge must separate two distinct faces.
(ix) The planar graphs that depict three-dimensional polyhedra are known as polyhedral graphs [47].

Considering i–ix, we can introduce Euler's second formula as part of his theorem of elementary mathematics [60–62]:

$$v + f - e = \chi \tag{23}$$

where χ denotes the Euler characteristic, a topological invariant that depends on the surface by taking into account the graph's genus g [60, 61]:

$$\chi = 2 - 2g \tag{24}$$

with $g = 0$ for the examples in Fig. 4. The column featuring $v + f - e$ in Table 1 illustrates the concept of this topological invariant for planar graphs. The genus g enables the generalization of graphs drawn on surfaces other than a plane [60]. If a graph is planar and satisfies Eq. (23), then it is connected [60]. Though there are relatively few instances of molecules exhibiting non-planar graphs [52,65], we can achieve topological generalization using Eqs. (23) and (24) for complex structures with a higher genus [47,50].

The handshaking lemma can be stated as [47]

$$\sum_{i=1}^{v} deg\left(v_i\right) = 2e \tag{25}$$

For buckminsterfullerene (**8**), where each of the 60 vertices ($v = 60$) has a degree of 3, the handshaking lemma provides $e = 3v/2 = 90$, which, through Eq. (23), results in $f = 2 + v/2 = 32$ (see Table 1).

It is striking that the majority of molecules are represented by planar graphs [52,65], including buckminsterfullerene. Before delving further, it is essential to clarify that non-planar molecules can be mathematically considered as planar graphs, a distinction rooted in mathematics (see distilled idea iv above). Essentially, the concept of structural complexity in chemistry should not be confused with that of planar graphs. The counting problem of partitioning the local mode parameters of a complete and non-redundant set was approached from the perspective of planar graphs. We then proposed an integration of Decius's formulas [7] with Euler's theorem [60–62] to derive the formulas already familiar to our group [16], generalizing them to describe polyhedral molecules for the first time in this Frontiers Article. The selection of the 9 diverse test molecules (see Fig. 1) aimed to illustrate that, despite their differing structural complexities, all molecules exhibit planar graphs. Additionally, the intention was to encompass representatives from the graph families: tree graphs (**1**–**3**), cycle graphs (**4** and **5**), and polyhedral graphs (**6**–**9**), thereby demonstrating the versatility and applicability of our generalized formulas for the counting problem.

3. Results and discussion

Within the realm of molecules, parameters such as bond lengths, angles, and dihedral angles function as internal coordinates. The clarification of the counting problem for partitioning local mode parameters of a complete and non-redundant set is organized as follows. The proposed planar graph approach is integrated into Decius's work [7] through Euler's polyhedral formula [60–62]. As previously stated, a planar graph is connected if it satisfies Eq. (23) [60].

Because LModeAGen satisfies Eq. (23), the issue with bond parameters associated with unphysical parameters is resolved, making the complete and non-redundant set generated by the new protocol chemically meaningful for local mode analysis. The problem that remains to be addressed is the search for optimal sets that minimize the vibrational coupling. ACS can detect such coupling in the form of a mismatch in the one-to-one relation between local and normal vibrational modes, and work is in progress towards a theoretical approach that utilizes CNM and another physical basis as a metric for determining the optimal sets.

3.1. Count of bond local mode parameters

Fig. 4 depicts representations of a tree, cycle, and polyhedral graph in a plane. The *infinite face*, discussed in Refs. [60,61], should be noted in these representations. Below is the discussion of the differentiation between faces and molecular cycles in more detail.

It is not difficult to demonstrate that when two graphs, A and B, of the types illustrated in Fig. 4, are connected by an edge, they still adhere to Euler's formula (Eq. (23)), as

$$(v_A + v_B) + (f_A + f_B - 1) - (e_A + e_B + 1) = 2 \tag{26}$$

The subscript indicates the respective quantities of individual components.

Graphs, as a concept rooted in a collection of objects with any notion of connection, can be readily extended to the realm of molecules, resulting in what we commonly refer to as molecular or chemical graphs, that is, graphs in the context of chemical topology [52]. This transition primarily involves adapting notations and terminology. Our primary objective is to generalize the formulas used to determine the number of local mode parameters in a molecule from a complete and non-redundant set. This set should adhere to conditions i to ix outlined earlier.

We begin by asserting that the very concept of completeness, which is well-known in our group within the context of local vibrational mode

theory [16,19], naturally arises from satisfying Euler's theorem [60–62]. Specifically, the total number of bond local mode parameters N_b corresponds to the total number of edges e in the molecular graph, while the total number of vertices v represents the total number of atoms N. Aside from polyhedral molecules, it should be noted that the number of molecular cycles N_c differs from the number of faces f by 1 thanks to the *infinite face*. Thus, the formula for predicting the number of bond local mode parameters in open-chain, cyclic, and cage-like structures representable in the plane can be extended through the application of Euler's formula (Eq. (23)):

$$N_b = N + f - 2 \tag{27}$$

with $N_c = f - 1$ for open-chain and cyclic molecules and $N_c = f$ for polyhedral molecules.

The requirement for connectivity, as outlined in our recently published local mode analysis protocol, LModeAGen [19], aligns with Eq. (26) and ensures the fulfillment of Euler's theorem [60–62]. Differences in connectivity can be translated into mathematics through the handshaking lemma (Eq. (25)), which sheds light on the significant discrepancy in the number of edges for the same number of vertices when progressing from a tree to a cycle or polyhedral graph, as depicted in Fig. 4. Table 1 demonstrates that the local mode parameters, automatically generated by LModeAGen [19], adhere to Euler's theorem [60–62] for planar graphs.

To emphasize connectivity, let us consider the cycle depicted in Fig. 4 as a hypothetical dimer composed of monomers 1–2–3–4 and 5–6–7–8, with the edges 1–8 and 4–5 representing non-covalent interactions, as we momentarily indulge in imagination. If one mistakenly connects either 1–8 or 4–5, not only does the topology of the graph change completely from a cycle to a tree, but the description of one non-covalent interaction will be omitted, resulting in a local vibrational space that fails to meet the requirements for a proper vibrational analysis of the problem through LModeAGen [19]. It is important to highlight that excluding both 1–8 and 4–5 results in a disconnected graph, failing to satisfy Euler's equation.

Altogether, the well-established concept of completeness in a chemically meaningful, non-redundant set of local vibrational modes can be viewed from the perspective of graph theory as a natural outcome of satisfying Euler's theorem for molecular graphs of tree, cycle, and polyhedral types. This marks a significant advancement by recognizing local vibrational mode theory from the perspective of graph theory for the first time. Ultimately, the elementary yet impactful mathematical ideas explored here substantiate our novel local mode analysis protocol, LModeAGen [19].

The partitioning problem extends beyond the discussion presented here, raising questions about how angles and dihedrals can be optimally divided to create a complete set of non-redundant bond, angle, and dihedral local vibrational modes that minimize coupling. Work is in progress to address this challenge. Meanwhile, we present preliminary formulas as follows for the number of angle and dihedral angle local mode parameters of plane graphs, building upon the foundations for linear and planar molecules laid by Decius [7]. We will revisit these formulas in a follow-up work while searching for optimal local mode sets that minimize vibrational coupling between the molecular fragments.

3.2. Count of angle and dihedral local mode parameters

3.2.1. Linear molecules

Linear molecules are depicted by a specific type of tree known as a path graph. According to Decius' prescription for linear molecules [7], the number of angle local mode parameters N_a can be determined as follows:

$$N_a = 2(N - 2) \tag{28}$$

The summation of Eqs. (28) and (27) results in $3N-5$ given that $f = 1$.

Table 1
Comparison of the total numbers of vertices (v), faces (f), and edges (e), alongside the manifestation of the topological invariant $v + f - e$, and the number of bond (N_b), angle (N_a), and dihedral (N_d) local mode parameters according to Eqs. (27), (28)–(30) (see text).

Examples		v	f	e	$v+f-e$	N_b	N_a	N_d
1	Acetylene	4	1	3	2	3	4	
2	Ethane	8	1	7	2	7	6	5
3	Glycine	10	1	9	2	9	8	7
4	Benzene	12	2	12	2	12	9	9
5	Bicyclo[2.2.2]octane	22	3	23	2	23	18	19
6	Cubane	16	6	20	2	20	9	13
7	Perfluorocubane	16	6	20	2	20	9	13
8	Buckminsterfullerene	60	32	90	2	90	27	57
9	Ar–benzene[a]	13			2			10

[a] The blank entries vary depending on the associated plane graph, which may have different connections concerning how the interaction between Ar and the benzene ring is depicted (see text).

3.2.2. Planar chemical graphs

From Decius' prescription for planar molecules [7], we can generalize the number of angle local mode parameters N_a and the total number of dihedral angle local mode parameters N_d for plane graphs using Eq. (27):

$$N_a = N - f - 1 \tag{29}$$

$$N_d = N - 3 \tag{30}$$

In our convention for dihedral angle parameters, any string with four elements represents a dihedral angle. Additionally, Eq. (27) enables us to rewrite Decius' quantity μ, with $\mu = N_b - N + 1$, as

$$\mu = f - 1 \tag{31}$$

To the best of our knowledge, this is the first time that μ has been recast in this manner. Herein, μ can be generalized to represent the number of edges that need to be removed to transform any planar graph, not just a cycle, into a tree. Eqs. (29) and (30) were derived by subtracting $3(f-1)$ from each type of parameter, corresponding to the 6μ redundancies in Decius' formulas [7]. Correction for the presence of linear submolecules is computed by adding $(l-1)$ to Eq. (29) and subtracting it from Eq. (30), with l representing the number of linear bonds [7].

Therefore, the formulas previously proposed in our group to obtain local mode results with chemical significance [16,19] can be retrieved. The generalization to polyhedral molecules, reported here for the first time within the scope of local mode analysis, adds a new dimension to our understanding.

3.3. A showcase of CNM

This section aims to showcase local mode analysis using CNM. Through CNM, it often becomes abundantly clear that normal vibrational modes fail to serve as an effective descriptor of bond strength due to delocalization [18,21]. In such cases, local vibrational modes come into play, offering a new perspective on vibrational analysis. Furthermore, the quantitative approach offered by CNM makes it possible to pinpoint the interacting functional groups when interpreting vibrational spectra [20].

3.3.1. Glycine

Glycine, despite its apparent simplicity, holds significant importance as it exemplifies how CNM works as a magnifying glass on vibrational fingerprints, probing structural and environmental changes. This can serve as a useful tool when scrutinizing IR spectra to provide reliable and consistent assignments. The CNM analysis shown here can be incorporated into a spectral analysis protocol extended to other amino

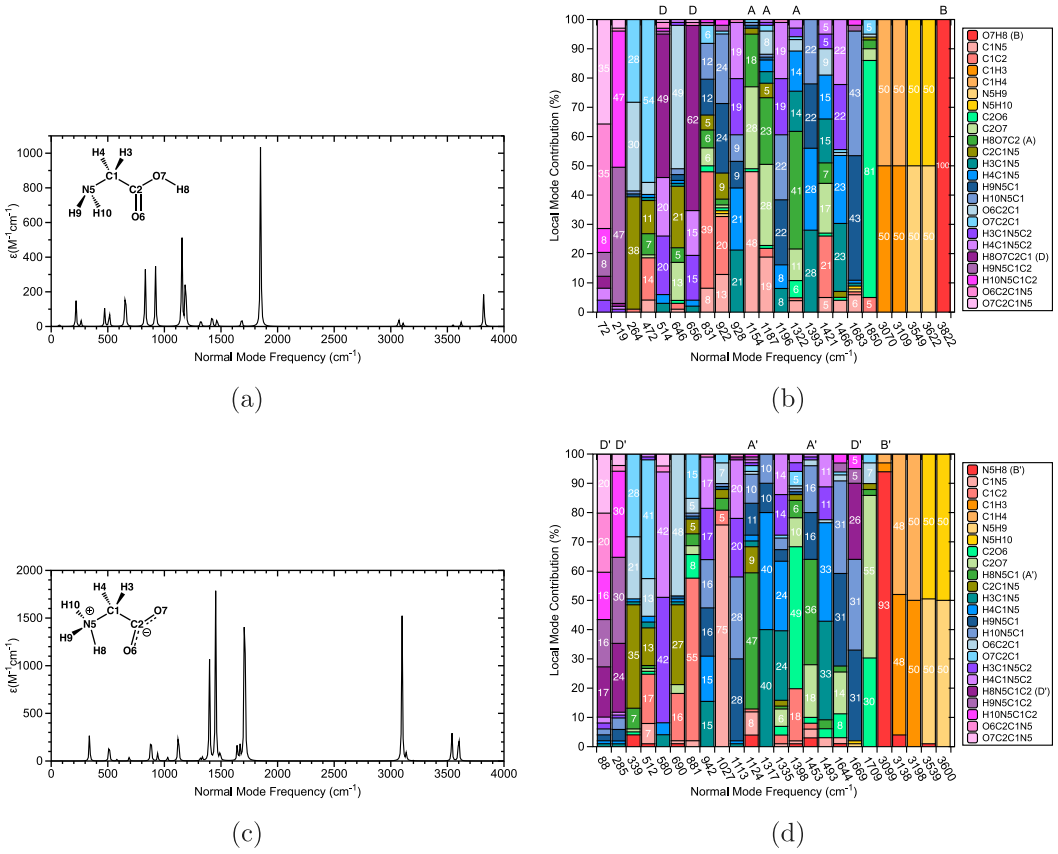

Fig. 5. CNM analysis of the canonical (b) and zwitterionic (d) forms of glycine at the ωB97X-D/aug-cc-pVTZ level of theory. The fingerprint fragments are indicated, and the calculated infrared spectra are provided for comparison.

acids, contributing to the debate on their presence in the interstellar medium [81].

Essentially, Fig. 5 provides a comprehensive analysis of the calculated normal vibrational modes, revealing distinct patterns associated with the characteristic interactions between fragments when transitioning from the canonical to the zwitterionic form, unveiling the localized nature of the normal vibrational modes of the O–H and N–H stretching vibrations, respectively. This analysis also presents a means to track down the local mode contributions due to the fragments that contain the hydrogen responsible for the structural changes (fingerprint fragments). Such fragments are indicated by B, A, and D for the bond, angle, and dihedral parameters containing H8. The prime symbol distinguishes those of the zwitterion.

In Fig. 5b, the fragments C1H3 and C1H4, as well as N5H9 and N5H10, equally contribute to the normal vibrational modes they form. Conversely, the normal vibrational modes of the zwitterion in Fig. 5d show some interaction between the N5H8, C1H3, and C1H4 fragments. This interaction is evident when examining the local mode frequencies associated with the fragments. While in the non-zwitterionic form, there are two degenerate N–H local mode frequencies at 3551 cm^{-1} and two degenerate C–H local mode frequencies at 3073 cm^{-1}, in the zwitterionic form, the quasi-degenerate C–H local mode frequencies occur at 3162 cm^{-1}, with the N5H8 local mode frequency occurring much closer, at 2905 cm^{-1}. The other N–H local mode frequencies, whose parameters are equivalent to those of the non-zwitterionic form, remain practically unchanged, occurring at 3562 cm^{-1}. Of particular interest is the probing of the interaction between the C–O fragments in both scenarios. From Fig. 5b to d, there is a clear increase in the coupling between the C–O fragments, with the normal vibrational modes occurring at 1398 and 1709 cm^{-1}. This can be understood due to the hydrogen transfer to the nitrogen atom, resulting in the local mode frequency values of C2O7 and C2O6 reaching 1582 and 1477 cm^{-1}, respectively, in the zwitterionic form. In the non-zwitterionic form, they occur at 1199 and 1791 cm^{-1}, respectively.

3.3.2. Cubane and perfluorocubane

Due to the dimension of the vibrational space, we have selectively analyzed only the normal vibrational modes supported by the vibrational spectra. Also, given the significant delocalization observed in the normal vibrational modes associated with the infrared-active peaks of both cubane and perfluorocubane, it is recommended to perform the CNM analysis using local mode families. For the C–H family, this entails aggregating all the percentage contributions of C–H local modes, $\sum_{j=1}^{8} C_j^{\%}(\mathrm{C-H})$, to form the C–H entry in Fig. 6. Similar rationale applies to other local mode families.

While the normal vibrational modes of cubane at 3141 cm^{-1} in Fig. 6b are collectively 99% localized with respect to the C–H local mode family, there is no equivalent for the C–F local mode family in perfluorocubane, as depicted in Fig. 6d. Instead, the C–F and C–C fragments are coupled in all the normal vibrational modes at 852 and 1431 cm^{-1}. The coupling between the C–C fragments and the X–C–C, X–C–C–C, and C–C–C–C fragments, where X represents H or F for cubane or perfluorocubane, respectively, is also evident.

3.3.3. Ar–benzene

The local modes S_x and S_y account for the lateral movement of A along the mean plane of the ring system B in two perpendicular directions, while S_z represents the actual stretching between the monomers A and B, reflecting their interaction [97]. In essence, S_x and S_y primarily ensure the completeness of the non-redundant vibrational space. However, as previously mentioned, a plane graph satisfying Eq. (23) implies that it is also connected [60]. Since Eqs. (27), (29), and (30) rely on Eq. (23), we had to devise an ansatz to ensure topological

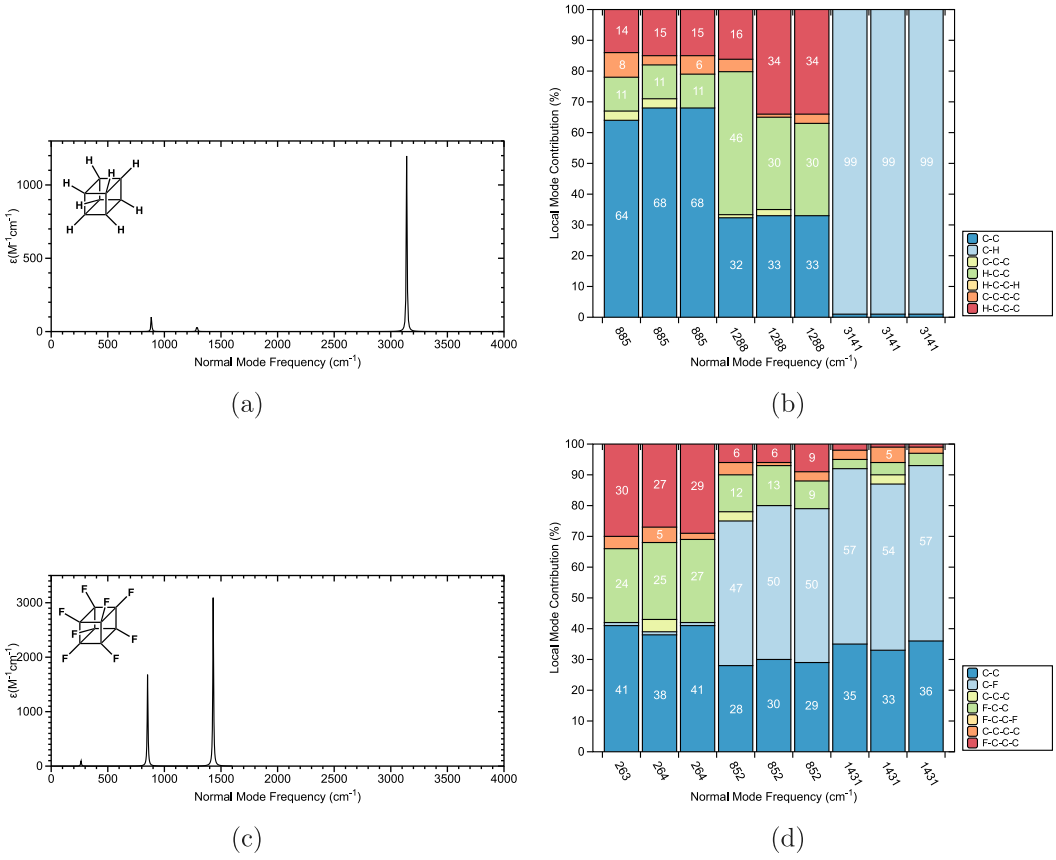

Fig. 6. CNM analysis of cubane (b) and perfluorocubane (d) at the ωB97X-D/aug-cc-pVTZ level of theory. The calculated infrared spectra are provided for comparison.

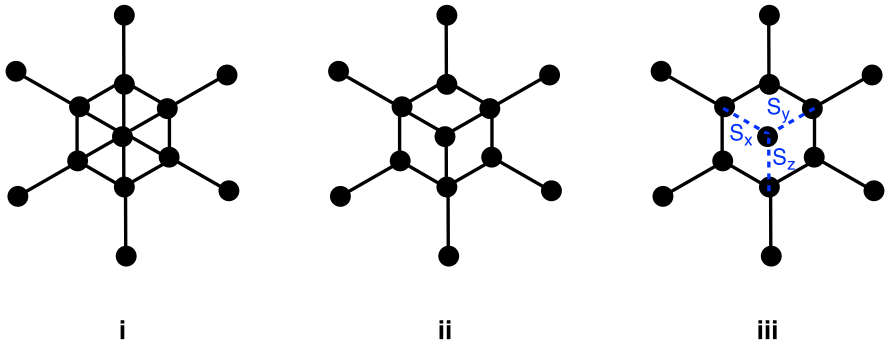

Fig. 7. Ansatz: (i) the plane graph containing all connections between the central vertex (Ar) and the vertices of the cycle (six-membered carbon ring), (ii) the plane graph where central edges (Ar–C bonds) can be replaced with S_x, S_y, and S_z, resulting in construct iii. This ansatz aims to reconcile our counting formulas with these special local modes for complete and non-redundant local mode sets.

consistency between LModeAGen and the special local modes regarding the counting problem we aimed to address in this Frontiers Article.

Fig. 7 demonstrates that when considering Ar–benzene (**9**), the thirteen vertices can be analyzed in different ways regarding the number of edges, faces, and the substitution of edges by the special local modes, all from a counting perspective. Graph i exhibits $N_b^i = 18$, $N_a^i = 5$, and $N_d^i = 10$, whereas graph ii displays $N_b^{ii} = 15$, $N_a^{ii} = 8$, and $N_d^{ii} = 10$. Evidently, these represent two distinct ways of partitioning $3N^{(9)} - 6 = 33$ local modes, with graph i featuring $f^i = 7$ and graph ii featuring $f^{ii} = 4$. The three intra-monomer stretching modes along the x-, y-, and z-directions, represented as S_x, S_y, and S_z, respectively, can substitute the three Ar–C bond local modes without altering the completeness and non-redundancy of the local mode set when transitioning from ii to iii. A comparative CNM analysis for i–iii is presented in Fig. 8.

Fig. 8 shows the CNM analysis of the normal vibrational modes linked to the infrared absorption peaks for the Ar-benzene dimer. The identical merging technique for local mode families, used in the cases of cubane and perfluorocubane, has been implemented here for the local modes unrelated to the π interaction. This highlights the focus on describing the interaction between Ar and the benzene ring. Although not explicitly shown in Fig. 8a, there exists a small peak at 81 cm^{-1} whose normal mode decomposition is significantly influenced by the selection of i, ii, or iii from the ansatz illustrated in Fig. 7. Notably, the choice does not impact the normal vibrational modes associated with C–H stretching vibrations, as they remain 99% collectively localized with respect to the C–H local mode family regardless of the option. However, there is a substantial variation in the local mode contributions for the normal vibrational modes in between when

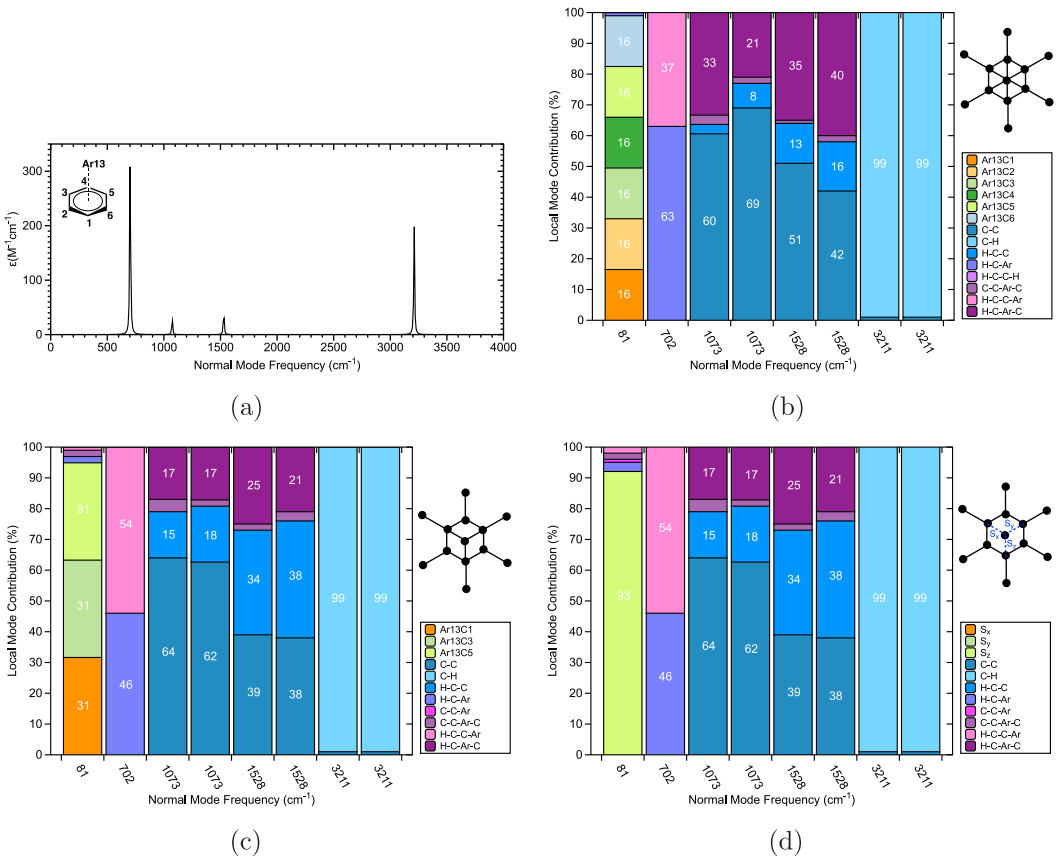

Fig. 8. CNM analysis of Ar-benzene at the ωB97X-D/aug-cc-pVTZ level of theory. The calculated infrared spectrum is provided for comparison. Ansatz: i (b), ii (c), and iii (d).

transitioning from i to ii, while CNM for iii remains unchanged next to ii except for the normal vibrational mode at 81 cm^{-1}. Construct iii effectively captures the decomposition of this normal vibrational mode, illustrating the interaction between Ar and the benzene ring, with 93% of localization due solely to S_z. The deficiencies of the CNM analysis for such normal vibrational mode, based on i and ii, have been demonstrated, along with the misleading local mode contributions within the frequency range of 702–1528 cm^{-1} when adopting graph i. Ultimately, the selection of special local modes combined with LModeAGen for Ar–benzene serves as a notable example, highlighting the absence of an optimization algorithm in current literature. This paves the way for the development of LModeAOPT, an algorithm aimed at generating an optimal local mode set by minimizing vibrational coupling.

4. Conclusion

This study has shed new light on the well-established concept of completeness in a chemically meaningful, non-redundant set of local vibrational modes by framing it within the realm of graph theory. Our exploration has revealed that this concept naturally emerges when Euler's theorem is satisfied for molecular graphs of various types, marking a significant milestone in our understanding of local vibrational mode theory.

This work supports our local mode analysis protocol, LModeAGen, by revealing the elementary yet impactful mathematical ideas that underpin it. Furthermore, we have highlighted the next step to addressing the partitioning problem in local mode analysis, an intriguing challenge that extends the discussion beyond this study. It prompts us to consider how angles and dihedrals can be optimally divided to create a complete set of non-redundant bond, angle, and dihedral local vibrational modes that minimizes coupling. This remains as an open problem with ongoing efforts in our group.

We have demonstrated the varying strengths of C–C bonds within a curated selection of organic compounds. Furthermore, we have showcased the local mode analysis, offering valuable insights into how CNM functions as a magnifying glass for vibrational fingerprints, allowing for the probing of structural and environmental changes.

We have combined the approach of special local modes with that of the new protocol of local mode analysis, LModeAGen, for the first time. This adaptation was guided by the topological insights presented in this Frontiers Article, aiming to consistently achieve a complete and non-redundant local mode set for the CNM analysis of dimeric systems such as the Ar–benzene dimer. In essence, the integration of special local modes with LModeAGen for Ar–benzene exemplifies a significant gap in current literature: the lack of an optimization algorithm. This lays the groundwork for the creation of LModeAOPT, an algorithm designed to produce an optimal local mode set by minimizing vibrational coupling.

CRediT authorship contribution statement

Mateus Quintano: Writing – original draft, Visualization, Validation, Software, Methodology, Investigation, Formal analysis, Data curation, Conceptualization. **Renaldo T. Moura Jr.:** Writing – review & editing, Validation, Methodology, Investigation, Formal analysis, Conceptualization. **Elfi Kraka:** Writing – review & editing, Validation, Supervision, Resources, Project administration, Methodology, Investigation, Funding acquisition, Conceptualization.

Declaration of competing interest

The authors declare the following financial interests/personal relationships which may be considered as potential competing interests: Elfi Kraka reports was provided by Southern Methodist University. Elfi Kraka reports a relationship with Southern Methodist University that includes: employment. There are no additional relationships or activities to declare.

Data availability

Data will be made available on request.

Acknowledgments

We thank SMU's Center for Research Computing for providing generous computational resources. We also thank Marek Freindorf for the comments and suggestions of great value. RTMJr thanks the Brazilian National Council for Scientific and Technological Development – CNPq, Grant numbers 406483/2023-0 and 310988/2023-3. MQ thanks SMU for the Postdoctoral Fellowship and Francielle Santos for the encouragement as well as the help with the conceptualization of the graphical abstract. This work was financially supported by the National Science Foundation, United States, Grant CHE 2102461.

References

[1] E. Kraka, W. Zou, Y. Tao, Decoding chemical information from vibrational spectroscopy data: Local vibrational mode theory, WIREs: Comput. Mol. Sci. 10 (2020) 1480.
[2] E. Kraka, M. Quintano, H.W. La Force, J.J. Antonio, M. Freindorf, The local vibrational mode theory and its place in the vibrational spectroscopy arena, J. Phys. Chem. A 126 (2022) 8781–8900.
[3] E.B. Wilson, Some mathematical methods for the study of molecular vibrations, J. Chem. Phys. 9 (1941) 76–84.
[4] E.B. Wilson, J.C. Decius, P.C. Cross, Molecular Vibrations: The Theory of Infrared and Raman Vibrational Spectra, McGraw-Hill, New York, 1955.
[5] Z. Konkoli, D. Cremer, A new way of analyzing vibrational spectra. I. Derivation of adiabatic internal modes, Int. J. Quantum Chem. 67 (1998) 1–9.
[6] D.L. Crittenden, Simple, near-universal relationships between bond lengths, strengths, and anharmonicities, AIP Adv. 13 (2023) 115323.
[7] J.C. Decius, Complete sets and redundancies among small vibrational coordinates, J. Chem. Phys. 17 (1949) 1315–1318.
[8] J. Baker, A. Kessi, B. Delley, The generation and use of delocalized internal coordinates in geometry optimization, J. Chem. Phys. 105 (1996) 192–212.
[9] W. Hug, M. Fedorovsky, Characterizing vibrational motion beyond internal coordinates, Theor. Chem. Account. 119 (2008) 113–131.
[10] K. Németh, M. Challacombe, M. Van Veenendaal, The choice of internal coordinates in complex chemical systems, J. Comput. Chem. 31 (2010) 2078–2086.
[11] N. Vaidehi, A. Jain, Internal coordinate molecular dynamics: A foundation for multiscale dynamics, J. Phys. Chem. B 119 (2015) 1233–1242.
[12] J. Li, O. Zhang, S. Lee, A. Namini, Z.H. Liu, J.a.M.C. Teixeira, J.D. Forman-Kay, T. Head-Gordon, Learning correlations between internal coordinates to improve 3D Cartesian coordinates for proteins, J. Chem. Theory Comput. 19 (2023) 4689–4700.
[13] M. Mendolicchio, J. Bloino, V. Barone, Perturb-then-diagonalize vibrational engine exploiting curvilinear internal coordinates, J. Chem. Theory Comput. 18 (12) (2022) 7603–7619.
[14] M. Mendolicchio, Harnessing the power of curvilinear internal coordinates: from molecular structure prediction to vibrational spectroscopy, Theor. Chem. Account. 142 (2023) 133.
[15] W. Zou, D. Cremer, C_2 in a box: Determining its intrinsic bond strength for the $X^1\ \Sigma_g^+$ ground state, Chem. Eur. J. 22 (2016) 4087–4097.
[16] W. Zou, R. Kalescky, E. Kraka, D. Cremer, Relating normal vibrational modes to local vibrational modes with the help of an adiabatic connection scheme, J. Chem. Phys. 137 (2012) 084114.
[17] M. Quintano, E. Kraka, Theoretical insights into the linear relationship between pK_a values and vibrational frequencies, Chem. Phys. Lett. 803 (2022) 139746–1–139746–7.
[18] R.T. Moura Jr., M. Quintano, C.V. Santos Jr., V.A. Albuquerque, E.C. Aguiar, E. Kraka, A.N. Carneiro Neto, Featuring a new computational protocol for the estimation of intensity and overall quantum yield in lanthanide chelates with applications to Eu(III) mercapto-triazole schiff base ligands, Opt. Mater. X 16 (2022) 100216–1–100216–15.
[19] R.T. Moura Jr., M. Quintano, J.J. Antonio, M. Freindorf, E. Kraka, Automatic generation of local vibrational mode parameters: From small to large molecules and QM/MM systems, J. Phys. Chem. A 126 (2022) 9313–9331.
[20] M. Quintano, A.A.A. Delgado, R.T. Moura Jr., M. Freindorf, E. Kraka, Local mode analysis of characteristic vibrational coupling in nucleobases and Watson–Crick base pairs of DNA, Electron. Struct. 4 (12) (2022) 044005–1–044005–17.
[21] M. Quintano, R.T. Moura Jr., E. Kraka, The pK_a rule in light of local mode force constants, Chem. Phys. Lett. 826 (2023) 140654–1–140654–7.
[22] M. Quintano, R.T. Moura Jr., E. Kraka, Exploring Jahn–Teller distortions: a local vibrational mode perspective, J. Mol. Model. 30 (2024) 102.
[23] K. Oenen, D.F. Dinu, K.R. Liedl, Determining internal coordinate sets for optimal representation of molecular vibration, J. Chem. Phys. 160 (2024) 014104.
[24] J.A. Boatz, M.S. Gordon, Decomposition of normal-coordinate vibrational frequencies, J. Phys. Chem. 93 (1989) 1819–1826.
[25] Z. Konkoli, J.A. Larsson, D. Cremer, A new way of analyzing vibrational spectra. II. Comparison of internal mode frequencies, Int. J. Quantum Chem. 67 (1998) 11–27.
[26] S.A. Corcelli, C.P. Lawrence, J.L. Skinner, Combined electronic structure/molecular dynamics approach for ultrafast infrared spectroscopy of dilute HOD in liquid H2O and D2O, J. Chem. Phys. 120 (2004) 8107–8117.
[27] B.M. Auer, J.L. Skinner, IR and Raman spectra of liquid water: Theory and interpretation, J. Chem. Phys. 128 (2008) 224511.
[28] M.D. Hanson, J.A. Readnour, A.A. Hassanali, S.A. Corcelli, Coupled local-mode approach for the calculation of vibrational spectra: Application to protonated water clusters, J. Phys. Chem. Lett. 12 (2021) 9226–9232.
[29] M.D. Hanson, S.A. Corcelli, Coupled local mode method for simulating vibrational spectroscopy, J. Chem. Phys. 157 (2022) 154103.
[30] J.J. Antonio, E. Kraka, Non-covalent π–interactions in mutated aquomet-Myoglobin proteins: A QM/MM and local vibrational mode study, Biochemistry 62 (2023) 2325–2337.
[31] M. Freindorf, J. Antonio, E. Kraka, Hydrogen sulfide ligation in hemoglobin I of lucina pectinata-a QM/MM and local mode study, J. Phys. Chem. A 127 (2023) 8316–8329.
[32] M. Freindorf, J.J. Antonio, E. Kraka, Iron–histidine bonding in bishistidyl hemoproteins-A local vibrational mode study, J. Comput. Chem. 45 (2024) 574–588.
[33] Y. Dangat, M. Freindorf, E. Kraka, Mechanistic insights into S-depalmitolyse activity of Cln5 protein linked to neurodegeneration and batten disease: A QM/MM study, J. Am. Chem. Soc. 146 (2024) 145–158.
[34] B.M.T.C. Peluzo, M.Z. Makoś, R.T. Moura Jr., M. Freindorf, E. Kraka, Linear versus bent uranium(II) metallocenes – A local vibrational mode study, Inorg. Chem. 62 (2023) 12510–12524.
[35] F. Bodo, A. Erba, E. Kraka, R.T. Moura Jr., Chemical bonding in uranium-based materials: A local vibrational mode case study of $Cs_2UO_2Cl_4$ and UCl_4 crystals, J. Comput. Chem. (2024) http://dx.doi.org/10.1002/jcc.27311.
[36] Y. Tao, W. Zou, S. Nanayakkara, M. Freindorf, E. Kraka, A revised formulation of the generalized subsystem vibrational analysis (GSVA), Theor. Chem. Acc. 140 (2021) 31–1–31–5.
[37] Y. Tao, C. Tian, N. Verma, W. Zou, C. Wang, D. Cremer, E. Kraka, Recovering intrinsic fragmental vibrations using the generalized subsystem vibrational analysis, J. Chem. Theory Comput. 14 (2018) 2558–2569.
[38] E. Estrada, What is a mathematician doing... in a chemistry class? Found. Chem. (2024) http://dx.doi.org/10.1007/s10698-023-09497-4.
[39] N. Pairault, F. Rizzi, D. Lozano, E.M.G. Jamieson, G.J. Tizzard, S.M. Goldup, A catenane that is topologically achiral despite being composed of oriented rings, Nature Chem. 15 (2023) 781–786.
[40] A.S. Baluna, A. Galan, D.A. Leigh, G.D. Smith, J.T.J. Spence, D.J. Tetlow, I.J. Vitorica-Yrezabal, M. Zhang, In search of wasserman's catenane, J. Am. Chem. Soc. 145 (2023) 9825–9833.
[41] J. Wang, Y. Ren, Y. Yang, X. Fan, B. Jiang, Z. Huang, J. Wang, Y. Yang, A graph theory assisted Monte Carlo algorithm for simulating the topology structure of LDPE and connection with molecular dynamics simulation, AIChE J. 69 (2023) e18111.
[42] A. Rezaee Javan, Y. Liu, Y.M. Xie, New families of cage-like structures based on goldberg polyhedra with non-isolated pentagons, J. Comput. Des. Eng. 10 (2023) 527–538.
[43] A. Smith, S. Runde, A.K. Chew, A.S. Kelkar, U. Maheshwari, R.C. Van Lehn, V.M. Zavala, Topological analysis of molecular dynamics simulations using the Euler characteristic, J. Chem. Theory Comput. 19 (2023) 1553–1567.
[44] B. Naskrecki, M. Jaskolski, Z. Dauter, The Euler characteristic as a basis for teaching topology concepts to crystallographers, J. Appl. Crystallogr. 55 (2022) 154–167.
[45] C.M.B. Machado, N.B.D. Lima, S.L.S. Lins, A.M. Simas, A theorized new class of polyhedral hydrocarbons of molecular formula CnHn and their bottom-up scaffold expansions into hyperstructures, Sci. Rep. 11 (2021) 5576.
[46] J.-i. Aihara, Graph theory of aromatic stabilization, Bull. Chem. Soc. Jpn. 89 (2016) 1425–1454.
[47] P. Schwerdtfeger, L.N. Wirz, J. Avery, The topology of fullerenes, WIREs Comput. Mol. Sci. 5 (2015) 96–145.
[48] S. Schein, J.M. Gayed, Fourth class of convex equilateral polyhedron with polyhedral symmetry related to fullerenes and viruses, Proc. Natl. Acad. Sci. USA 111 (2014) 2920–2925.
[49] K.K. Baldridge, J.S. Siegel, Of graphs and graphenes: Molecular design and chemical studies of aromatic compounds, Angew. Chem. Int. Edn 52 (2013) 5436–5438.
[50] C. Chuang, Y. Fan, B. Jin, Systematics of toroidal, helically-coiled carbon nanotubes, high-genus fullernens, and other exotic graphitic materials, Procedia Eng. 14 (2011) 2373–2385.
[51] G.A. Breault, C.A. Hunter, P.C. Mayers, Supramolecular topology, Tetrahedron 55 (1999) 5265–5293.

[52] J.-C. Chambron, D.K. Mitchell, Chemical topology: The ins and outs of molecular structure, J. Chem. Educ. 72 (1995) 1059.
[53] H.L. Frisch, E. Wasserman, Chemical topology, J. Am. Chem. Soc. 83 (1961) 3789–3795.
[54] W. Xu, Y. Nagata, N. Kumagai, TEtraQuinolines: A missing link in the family of porphyrinoid macrocycles, J. Am. Chem. Soc. 145 (2023) 2609–2618.
[55] A. Weingarten, Rings of power, Nature Chem. 15 (2023) 453.
[56] P.E. Eaton, T.W. Cole, Cubane, J. Am. Chem. Soc. 86 (1964) 3157–3158.
[57] H.W. Kroto, J.R. Heath, S.C. O'Brien, R.F. Curl, R.E. Smalley, C60: Buckminsterfullerene, Nature 318 (1985) 162–163.
[58] M. Sugiyama, M. Akiyama, Y. Yonezawa, K. Komaguchi, M. Higashi, K. Nozaki, T. Okazoe, Electron in a cube: Synthesis and characterization of perfluorocubane as an electron acceptor, Science 377 (2022) 756–759.
[59] M.P. Krafft, J.G. Riess, About perfluoropolyhedranes, their electron-accepting ability and questionable supramolecular hosting capacity, Angew. Chem. Int. Edn 62 (2023) e202302942.
[60] R.J. Trudeau, Introduction to Graph Theory, Dover Pub., 1993.
[61] Euler's Polyhedral Formula, American Mathematical Society (AMS), 2004, URL ams.org/publicoutreach/feature-column/fcarc-eulers-formula.
[62] R. Grassl, O. Levin, More discrete mathematics: via graph theory, 2023, URL discrete.openmathbooks.org/more/mdm/sec_planar.html. (Accessed 27 September 2023).
[63] M. Harig, B. Neumann, H.-G. Stammler, D. Kuck, An elusive nonaromatic goal behind the centropolyindanes: Aufbau of veratrolo-annelated centropolyquinanes and ozonolytic abbau, ChemPlusChem 82 (2017) 1078–1095.
[64] D. Kuck, Molecules with Nonstandard Topological Properties: Centrohexaindane, Kuratowski's Cyclophane and Other Graph-Theoretically Nonplanar Molecules, John Wiley & Sons, Ltd, 2009, pp. 425–447, (Chapter 9).
[65] C. Rücker, M. Meringer, How many organic compounds are graph-theoretically nonplanar? MATCH Commun. Math. Comput. Chem. 45 (2002).
[66] E.E. Fenlon, Double, double trefoil and trouble, Nat. Synth. 1 (2022) 586–587.
[67] Z. Ashbridge, S.D.P. Fielden, D.A. Leigh, L. Pirvu, F. Schaufelberger, L. Zhang, Knotting matters: orderly molecular entanglements, Chem. Soc. Rev. 51 (2022) 7779–7809.
[68] F. Schaufelberger, Open questions in functional molecular topology, Commun. Chem. 3 (2020) 182.
[69] E.E. Fenlon, What tangled webs we weave, Nature Chem. 10 (2018) 1078–1079.
[70] S.D.P. Fielden, D.A. Leigh, S.L. Woltering, Molecular knots, Angew. Chem. Int. Edn 56 (2017) 11166–11194.
[71] E.E. Fenlon, Open problems in chemical topology, Eur. J. Org. Chem. 2008 (2008) 5023–5035.
[72] G.-Y. Qiao, X. Wang, X. Li, J. Li, K. Geng, E. Jin, J.-J. Xu, J. Yu, Unlocking synthesis of polyhedral oligomeric silsesquioxane-based three-dimensional polycubane covalent organic frameworks, J. Am. Chem. Soc. 146 (2024) 3373–3382.
[73] X. Chang, Y. Xu, M. von Delius, Recent advances in supramolecular fullerene chemistry, Chem. Soc. Rev. 53 (2024) 47–83.
[74] Y. Li, H. Jiang, W. Zhang, X. Zhao, M. Sun, Y. Cui, Y. Liu, Hetero- and homointerlocked metal-organic cages, J. Am. Chem. Soc. 146 (2024) 3147–3159.
[75] D.V. Khakimov, I.V. Svitanko, T.S. Pivina, Computational insight into the crystal structures of cubane and azacubanes, J. Mol. Model. 30 (2024) 93.
[76] T. Cao, Q. Meng, Z. Fu, Y. Shen, Y. Yan, Q. Wang, B. Zhao, W. Wang, K. Merimi, A. Rodríguez-Fortea, Y.-R. Yao, N. Chen, Th@C2(8)-C84 and Th@Cs(15)-C84: impact of actinide metal ions on the electronic structures of actinide endohedral metallofullerenes, Inorg. Chem. Front. 10 (2023) 6901–6908.
[77] Y.-R. Yao, J. Zhao, Q. Meng, H.-S. Hu, M. Guo, Y. Yan, J. Zhuang, S. Yang, S. Fortier, L. Echegoyen, W.H.E. Schwarz, J. Li, N. Chen, Synthesis and characterization of U≡C triple bonds in fullerene compounds, J. Am. Chem. Soc. 145 (2023) 25440–25449.
[78] W. Xue, T.K. Ronson, Z. Lu, J.R. Nitschke, Solvent drives switching between Λ and Δ metal center stereochemistry of M_8L_6 cubic cages, J. Am. Chem. Soc. 144 (2022) 6136–6142.
[79] L. Yang, B. Li, X. Gu, K. Niu, P. Jin, Discovery of non-isolated-pentagon-rule fullerenes from computational characterization of U2O@C72, Inorg. Chem. 60 (2021) 6492–6502.
[80] F. Pichierri, Substituent effects in cubane and hypercubane: a DFT and QTAIM study, Theor. Chem. Acc. 136 (2017) 114.
[81] R.L. Hudson, Interstellar tryptophan revisited, Mon. Not. R. Astron. Soc. 526 (2023) 4051–4053.
[82] T. Carl, E.S. Wirström, P. Bergman, S.B. Charnley, Y.-L. Chuang, Y.-J. Kuan, Deep search for glycine conformers in barnard 5, Mon. Not. R. Astron. Soc. 524 (2023) 5993–6003.
[83] V.M. Rivilla, M. Sanz-Novo, I. Jiménez-Serra, et al., First glycine isomer detected in the interstellar medium: Glycolamide (NH2C(O)CH2OH), Astrophys. J. Lett. 953 (2023) L20.
[84] R.C. Fortenberry, A vision for the future of astrochemistry in the interstellar medium by 2050, ACS Phys. Chem. Au 4 (2024) 31–39.
[85] J. Bowles, S. Jähnigen, R. Vuilleumier, F. Calvo, C. Clavaguéra, F. Agostini, Influence of the environment on the infrared spectrum of alanine: An effective mode analysis, J. Chem. Phys. 158 (2023) 094305.
[86] R.F.W. Bader, Atoms in Molecules: A Quantum Theory, Clarendon Press, Oxford, 1994.
[87] M.J. Frisch, G.W. Trucks, H.B. Schlegel, G.E. Scuseria, M.A. Robb, J.R. Cheeseman, G. Scalmani, V. Barone, G.A. Petersson, H. Nakatsuji, et al., Gaussian 16 Revision C.01, Gaussian Inc., Wallingford CT, 2016.
[88] J.-D. Chai, M. Head-Gordon, Long-range corrected hybrid density functionals with damped atom–atom dispersion corrections, Phys. Chem. Chem. Phys. 10 (2008) 6615–6620.
[89] T.H. Dunning, Gaussian basis sets for use in correlated molecular calculations. I. The atoms boron through neon and hydrogen, J. Chem. Phys. 90 (1989) 1007–1023.
[90] R.A. Kendall, T.H. Dunning, R.J. Harrison, Electron affinities of the first-row atoms revisited. Systematic basis sets and wave functions, J. Chem. Phys. 96 (1992) 6796–6806.
[91] J. Tomasi, B. Mennucci, R. Cammi, Quantum mechanical continuum solvation models, Chem. Rev. 105 (2005) 2999–3094.
[92] E.C. Meng, T.D. Goddard, E.F. Pettersen, G.S. Couch, Z.J. Pearson, J.H. Morris, T.E. Ferrin, UCSF chimeraX: Tools for structure building and analysis, Protein Sci. 32 (2023) e4792.
[93] W. Zou, R. Moura Jr., M. Quintano, F. Bodo, Y. Tao, M. Freindorf, M.Z. Makoś, N. Verma, D. Cremer, E. Kraka, LModeA2023, Computational and Theoretical Chemistry Group (CATCO), Southern Methodist University, Dallas, TX, USA, 2023.
[94] D. Cremer, E. Kraka, From molecular vibrations to bonding, chemical reactions, and reaction mechanism, Curr. Org. Chem. 14 (2010) 1524–1560.
[95] E. Kraka, J.A. Larsson, D. Cremer, Generalization of the badger rule based on the use of adiabatic vibrational modes, in: J. Grunenberg (Ed.), Computational Spectroscopy, Wiley, New York, 2010, pp. 105–149.
[96] V.P. Oliveira, B.L. Marcial, F.B. Machado, E. Kraka, Relating bond strength and nature to the thermodynamic stability of hypervalent togni-type iodine compounds, ChemPlusChem 86 (2021) 1199–1210.
[97] W. Zou, M. Freindorf, V. Oliveira, Y. Tao, E. Kraka, Weak and strong π interactions between two monomers – assessed with local vibrational mode theory, Can. J. Chem. 101 (2023) 616–632.
[98] A. Madushanka, R.T. Moura Jr., N. Verma, E. Kraka, Quantum mechanical assessment of protein–ligand hydrogen bond strength patterns: Insights from semiempirical tight-binding and local vibrational mode theory, Int. J. Mol. Sci. 24 (2023) 6311–1–6311–24.
[99] E. Kraka, M. Freindorf, Characterizing the metal ligand bond strength via vibrational spectroscopy: The metal ligand electronic parameter (MLEP), in: A. Lledós, G. Ujaque (Eds.), Topics in Organometallic Chemistry - New Directions in the Modeling of Organometallic Reactions, vol. 67, Springer, Berlin, Heidelberg, 2020, pp. 1–43, eBook.
[100] M. Freindorf, E. Kraka, Critical assessment of the FeC and CO bond strength in carboxymyoglobin - A QM/MM local vibrational mode study, J. Mol. Model. 26 (2020) 281–1–281–15.
[101] M. Freindorf, A.A.A. Delgado, E. Kraka, CO bonding in hexa– and pentacoordinate carboxy–neuroglobin – A QM/MM and local vibrational mode study, J. Comput. Chem. 43 (2022) 1725–1746.
[102] Z. Konkoli, D. Cremer, A new way of analyzing vibrational spectra. III. Characterization of normal vibrational modes in terms of internal vibrational modes, Int. J. Quantum Chem. 67 (1998) 29–40.

Mateus Quintano obtained his Ph.D. in Theoretical and Computational Chemistry from Southern Methodist University in 2023, following his B.S. and M.S. degrees in Chemistry from the Federal University of Minas Gerais, Brazil, in 2018 and 2020, respectively. Currently, he serves as a postdoctoral fellow in the CATCO research group at Southern Methodist University. His career path has been marked by research interests in theoretical physical chemistry, with a focus on vibrational spectroscopy, statistical thermodynamics, and mathematical methods.

Renaldo T. Moura Jr. received his Ph.D. from the Federal University of Pernambuco (Universidade Federal de Pernambuco – UFPE, Brazil) in 2013. Following that, he served as a postdoctoral fellow from 2013 to 2016 at the Department of Fundamental Chemistry (Departamento de Química Fundamental – dQF – UFPE, Brazil). Since 2016, he has held the position of Assistant Professor at the Department of Chemistry and Physics (Departamento de Química e Física) at the Federal University of Paraíba (Universidade Federal da Paraíba), located in João Pessoa, PB, Brazil. During the academic years of 2022 to 2023, he served as a Visiting Professor at the Computational and Theoretical Chemistry Group (CATCO) at Southern Methodist University (SMU) in Dallas, Texas, USA. Prior to this, he held the role of chair of the Department of Chemistry and Physics from 2019 to 2022. Prof. Renaldo's research interests focus on the development of theoretical and computational methods within the fields of inorganic and physical chemistry, with a particular emphasis on numerical methods, chemical bonding, and molecular spectroscopy. Throughout his career, he has supervised and co-supervised 3 Ph.D., 11 M.Sc., and 17 undergraduate students. Presently, he is supervising and co-supervising 4 Ph.D. and supervising 2 M.Sc. students. He has authored 4 book chapters and approximately 42 papers in journals with significant impact factors.

Elfi Kraka is Dedman Family Distinguished Professor and Harold A. Jeskey Endowed Chair of Chemistry at Southern Methodist University (SMU), Dallas. From 2005–2009 she was Full Professor of Chemistry and Department Chair at the University of the Pacific, Stockton, CA, and from 1990–2005 she rose through the ranks from Assistant to Full Professor at the University of Göteborg, Sweden. She served at SMU as Department Chair from 2009–2023. Since 2017 she is the Head of SMU's Computational and Theoretical Chemistry group (CATCO). She received the Doctor *rerum naturalis* in Theoretical Chemistry at the University of Cologne, Germany in 1985 with *summa cum laude*. CATCO's research mission is to develop modern quantum chemical tools and apply these tools to solve pending problems in chemistry, biology, materials science, and beyond. Current research topics stretch from catalysis, vibrational spectroscopy to machine learning supported computer assisted drug design. She has published more than 265 peer-refereed articles and presented her research at about 160 international conferences. She is a member of the Scientific Board of the World Association of Theoretical and Computational Chemists (WATOC) and serves on several Editorial Boards.